arXiv:1006.1164v2 [hep-lat] 10 Jun 2010

UTHEP-609
UTCCS-P-59

Non-perturbative renormalization of quark mass in $N_f = 2 + 1$ QCD with the Schrödinger functional scheme

S. Aoki[1,2], K. -I. Ishikawa[3], N. Ishizuka[1,2], T. Izubuchi[4],
K. Kanaya[1], Y. Kuramashi[1,2], K. Murano[1], Y. Namekawa[2],
M. Okawa[3], Y. Taniguchi[1,2], A. Ukawa[2], N. Ukita[2] and T. Yoshié[1,2]
(PACS-CS collaboration)

[1]*Graduate School of Pure and Applied Sciences,*
University of Tsukuba, Tsukuba, Ibaraki 305-8571, Japan
[2]*Center for Computational Physics,*
University of Tsukuba, Tsukuba, Ibaraki 305-8577, Japan
[3]*Graduate School of Science, Hiroshima University,*
Higashi-Hiroshima, Hiroshima 739-8526, Japan
[4]*Riken BNL Research Center, Brookhaven National*
Laboratory, Upton, New York 11973, USA

(Dated: June 11, 2010)

Abstract

We present an evaluation of the quark mass renormalization factor for $N_f = 2 + 1$ QCD. The Schrödinger functional scheme is employed as the intermediate scheme to carry out non-perturbative running from the low energy region, where renormalization of bare mass is performed on the lattice, to deep in the high energy perturbative region, where the conversion to the renormalization group invariant mass or the $\overline{\text{MS}}$ scheme is safely carried out. For numerical simulations we adopted the Iwasaki gauge action and non-perturbatively improved Wilson fermion action with the clover term. Seven renormalization scales are used to cover from low to high energy regions and three lattice spacings to take the continuum limit at each scale. The regularization independent step scaling function of the quark mass for the $N_f = 2 + 1$ QCD is obtained in the continuum limit. Renormalization factors for the pseudo scalar density and the axial vector current are also evaluated for the same action and the bare couplings as two recent large scale $N_f = 2 + 1$ simulations; previous work of the CP-PACS/JLQCD collaboration, which covered the up-down quark mass range heavier than $m_\pi \sim 500$ MeV and that of PACS-CS collaboration for much lighter quark masses down to $m_\pi = 155$ MeV. The quark mass renormalization factor is used to renormalize bare PCAC masses in these simulations.

I. INTRODUCTION

The strong coupling constant and the quark masses constitute the fundamental parameters of the Standard Model. It is an important task of lattice QCD to determine these parameters using inputs at low energy scales such as hadron masses, meson decay constants and heavy quark potential quantities. The results can be compared with independent determinations from high energy experiments.

In the course of evaluating these fundamental parameters we need the process of renormalization in some scheme. The $\overline{\mathrm{MS}}$ scheme is one of the most popular schemes, and hence one would like to evaluate the running coupling constant and quark masses through input of low energy quantities on the lattice and convert it to the $\overline{\mathrm{MS}}$ scheme. A difficulty in this process is that the conversion is given only in a perturbative expansion, and should be performed at much higher energy scales than the QCD scale. At the same time the renormalization scale μ should be kept much smaller than the lattice cut-off to reduce lattice artifacts. Furthermore we may need to suppress artifacts due to a finite lattice extension L. We therefore require

$$\frac{1}{L} \ll \Lambda_{\mathrm{QCD}} \ll \mu \ll \frac{1}{a}. \tag{I.1}$$

The practical difficulty of satisfying these inequalities in numerical simulations is called the window problem.

The Schrödinger functional (SF) scheme [1–9] is designed to solve the window problem. It has an advantage that systematic errors can be unambiguously controlled. A unique renormalization scale is introduced through the box size L in the chiral limit and the scheme is mass independent. A wide range of renormalization scales can be covered by the step scaling function (SSF) technique. This matches our goal to obtain the coupling constant and quark masses in the $\overline{\mathrm{MS}}$ scheme. The SF scheme has been applied for evaluation of the QCD coupling for $N_f = 0$ [2], $N_f = 2$ [7] and $N_f = 2 + 1$ [9] cases.

For the quark mass renormalization factor the SF scheme has been applied for $N_f = 0$ [5] and $N_f = 2$ [8] QCD. At low energy scales of $\mu \sim 500$ MeV, where physical input is given, we expect the strange quark contribution to be important in addition to those of the up and down quarks. Thus the aim of the present paper is to go one step further and evaluate the quark mass renormalization factor in $N_f = 2 + 1$ QCD. Our goal is to renormalize the bare light quark masses and meson decay constants evaluated in two recent large-scale $N_f = 2 + 1$ lattice QCD simulations employing non-perturbatively O(a) improved Wilson quark action; the work of CP-PACS/JLQCD Collaboration with relatively heavy pion mass of $m_\pi \sim 500$ MeV [10] and that of PACS-CS collaboration with much lighter quark masses down to $m_\pi = 155$ MeV [11, 12].

II. OUR STRATEGY

Our goal is to evaluate the renormalization group invariant (RGI) quark mass M given by

$$M = \overline{m}(\mu) \left(2b_0 \overline{g}^2(\mu)\right)^{-\frac{d_0}{2b_0}} \exp\left(-\int_0^{\overline{g}(\mu)} dg \left(\frac{\tau(g)}{\beta(g)} - \frac{d_0}{b_0 g}\right)\right), \tag{II.1}$$

where $\overline{g}(\mu)$ and $\overline{m}(\mu)$ are renormalized coupling and quark mass in some scheme at scale μ. $\beta(g)$ and $\tau(g)$ are the renormalization group (RG) function of coupling and mass in the same scheme.

Once the RGI mass M, which is scheme independent, is evaluated, the conversion into the $\overline{\mathrm{MS}}$ scheme can be carried out from the equation (II.1) with the RG functions in the $\overline{\mathrm{MS}}$ scheme.

We therefore first derive the renormalization factor $Z_M(g_0)$, which converts the bare PCAC mass at a bare coupling g_0 to the RGI mass. Since the step scaling function (SSF) $\sigma(u)$ for the running coupling has already been obtained[9], an evaluation of the RGI mass renormalization factor proceeds in the same way as given in Ref. [5, 8], which we briefly summarize here.

1. We start by preparing the coupling step scaling function $\sigma(u)$, which gives the relation between the renormalized coupling constants when the renormalization scale is changed by a factor two,

$$\sigma\left(u\right)=\lim_{a\to 0}\left(\overline{g}^2(2L)\Big|_{u=\overline{g}^2(L),m=0}\right). \tag{II.2}$$

   The renormalization scale is defined through a physical box size L where the renormalized coupling $u=\overline{g}^2(L)$ is evaluated in the SF scheme.

2. We define a reference scale L_{max} through a renormalized coupling constant $u_0=\overline{g}^2(L_{\mathrm{max}})$. The value of u_0 is arbitrary as long as it is well in the low energy region to suppress lattice artifacts with $a/L_{\mathrm{max}}\ll 1$ and within the range covered by the SSF. We need some physical input measured separately in simulation at large volume to evaluate L_{max} in physical units. In this paper we shall adopt the lattice spacing determined from hadron masses for this purpose.

3. We then calculate the step scaling function (SSF) Σ_P for the pseudo scalar density, which is given by the ratio of two renormalization factors at different renormalization scales $\mu=1/L$ and $1/(2L)$ at the same bare coupling g_0

$$\Sigma_P\left(u,\frac{a}{L}\right)=\left.\frac{Z_P(g_0,a/(2L))}{Z_P(g_0,a/L)}\right|_{\overline{g}^2(L)=u,m=0}, \tag{II.3}$$

   where mass independent scheme in the massless limit is adopted. We used the same definition of the pseudo scalar density renormalization factor Z_P as Ref. [5, 8].

   After taking the continuum limit with three lattice spacings

$$\lim_{a\to 0}\Sigma_P\left(u,\frac{a}{L}\right)=\sigma_P(u) \tag{II.4}$$

   and performing a polynomial fit for $\sigma_P(u)$ we get the non-perturbative renormalization group flow of the quark mass.

4. Since the SSF $\sigma_P(u)$ is given as a function of renormalized coupling u we need to prepare a sequence of couplings u_i in order to perform a non-perturbative running starting from $u_0=\overline{g}^2(L_{\mathrm{max}})$. u_i's differ by a factor two in the renormalization scale $L_i=2^{-i}L_{\mathrm{max}}$ and is given by solving the SSF $\sigma(u_{i+1})=u_i$. We find that we are well in the perturbative region for $i\geq 5$ [9].

5. Taking the product of the SSF $\sigma_P(u_i)$ at each scale we get a factor

$$\frac{\overline{m}(1/L_n)}{\overline{m}(1/L_{\rm max})} = w_n^{-1} = \prod_{i=1}^{n} \sigma_P(u_i) \tag{II.5}$$

which represents the running of the renormalized mass from $L_{\rm max}$ to L_n. We derive the renormalization factor, which converts the quark mass in the SF scheme at the reference scale $L_{\rm max}$ to the RGI mass

$$\frac{M}{\overline{m}(1/L_{\rm max})} = \frac{\overline{m}(1/L_n)}{\overline{m}(1/L_{\rm max})}\frac{M}{\overline{m}(1/L_n)} = w_n^{-1}\frac{M}{\overline{m}(1/L_n)}. \tag{II.6}$$

The last factor $M/\overline{m}(1/L_n)$ is evaluated perturbatively for $n \geq 5$ with $\tau(g)$ at two-loop order and $\beta(g)$ at three-loop order [19] using (II.1).

6. The renormalized PCAC quark mass at scale $\mu = 1/L_{\rm max}$ is given by

$$\overline{m}(1/L_{\rm max}) = \lim_{a\to 0} \frac{Z_A(g_0, a/L)}{Z_P(g_0, a/L_{\rm max})}\, m_{\rm PCAC}^{\rm (bare)}(g_0). \tag{II.7}$$

The bare PCAC quark mass $m_{\rm PCAC}^{\rm (bare)}(g_0)$ is obtained in some simulation at large volume carried out at a bare coupling g_0. We need to calculate the renormalization factor $Z_A(g_0, a/L)$ for the axial current [22, 23] and $Z_P(g_0, a/L_{\rm max})$ for the pseudo scalar density at the same bare coupling g_0 in this simulation. The box size L for the axial current need not coincide with the box size $L_{\rm max}$ for the pseudo scalar density since the former is scale independent in the continuum limit. We finally obtain

$$Z_M(g_0, a/L_{\rm max}) = \frac{M}{\overline{m}(1/L_{\rm max})}\ \frac{Z_A(g_0, a/L)}{Z_P(g_0, a/L_{\rm max})}. \tag{II.8}$$

The factor $Z_A(g_0, a/L)$ is also used for renormalization of meson decay constants.

7. As a last step, we evaluate the mass renormalization factor in $\overline{\rm MS}$ scheme at a scale μ:

$$Z_m^{\overline{\rm MS}}(g_0, \mu) = \frac{\overline{m}_{\overline{\rm MS}}(\mu)}{M} Z_M(g_0, a/L_{\rm max}) \tag{II.9}$$

The factor $\overline{m}_{\overline{\rm MS}}(\mu)/M$ is given by using (II.1) with the renormalization group functions in $\overline{\rm MS}$ scheme at four loops. The renormalization scale μ is introduced through the RGI scale $\Lambda_{\overline{\rm MS}}$ evaluated in Ref. [9].

III. NUMERICAL SETUPS

We adopt the renormalization group improved Iwasaki gauge action and the $\mathcal{O}(a)$ improved Wilson fermion action with the clover term, whose parameters are identical to those adopted in the previous paper for the running coupling [9]: The boundary improvement coefficients of the gauge action are set to the tree-level values $c_{\rm t}^P = 1$ and $c_{\rm t}^R = 3/2$ for Iwasaki action [13]. The improvement coefficient $c_{\rm SW}$ of the clover term is known non-perturbatively [14]. The boundary improvement coefficient $\tilde{c}_t$ of the fermion action is set to the one loop value [15]. Differences reside in the Dirichlet boundary condition for the spatial gauge link, which is set to

$$U_k(x)|_{x_0=0} = U_k(x)|_{x_0=T} = \begin{pmatrix} 1 & & \\ & 1 & \\ & & 1 \end{pmatrix} \tag{III.1}$$

and the twisted periodic boundary condition of the fermion fields in the three spatial directions

$$\psi(x + L\hat{k}) = e^{i\theta}\psi(x), \quad \overline{\psi}(x + L\hat{k}) = e^{-i\theta}\overline{\psi}(x), \tag{III.2}$$

where $\theta = 0.5$ [5, 8]. These conditions are known to show a good perturbative behavior [16] for the quark mass renormalization factor.

For numerical simulations, the HMC algorithm is adopted for up and down quarks and the RHMC algorithm for the strange quark. The masses of all three quarks are set to zero. We adopt the CPS++ code [17] and add some modification for the SF formalism. Simulations were carried out mainly on the T2K-tsukuba computer at University of Tsukuba and the T2K-tokyo computer at University of Tokyo [18].

IV. STEP SCALING FUNCTION

A. Pseudo scalar density renormalization factor

We adopt seven renormalized coupling values to cover weak ($\overline{g}^2 = 1.001$) to strong ($\overline{g}^2 = 3.418$) coupling regions [9], which approximately satisfy $\overline{g}^2_{i+1}(L) = \overline{g}^2_i(2L)$. For each coupling we use three box sizes $L/a = 4, 6, 8$ to take the continuum limit. At the three lattice sizes the values of β and κ were tuned to reproduce the same renormalized coupling keeping the PCAC mass to zero. On the same parameters we evaluate the pseudo scalar density renormalization factor $Z_P(g_0, a/L)$ and $Z_P(g_0, a/(2L))$ with the Dirichlet boundary condition (III.1).

We adopt the definition of the renormalization factor [5, 8] given by

$$Z_P(g_0, a/L) = \frac{1}{n_P}\frac{\sqrt{N_c f_1}}{f_P(L/2)}, \tag{IV.1}$$

where $f_P(x_0)$ and f_1 are two-point functions of pseudo scalar density at bulk and at boundary given by

$$f_P(x_0) = -\frac{1}{N_f^2 - 1}\frac{a^3}{L^3}\sum_{\vec{x}} \langle P^a(x)\mathcal{O}^a \rangle, \tag{IV.2}$$

$$f_1 = -\frac{1}{N_f^2 - 1}\frac{a^6}{L^6} \langle \mathcal{O}'^a\mathcal{O}^a \rangle, \tag{IV.3}$$

$$P^a(x) = \overline{\psi}(x)\gamma_5\frac{1}{2}\tau^a\psi(x). \tag{IV.4}$$

The boundary pseudo scalar operators $\mathcal{O}^a$ and $\mathcal{O}'^a$ are written in terms of the boundary quark fields ζ, $\overline{\zeta}$, ζ', $\overline{\zeta}'$ [4] as

$$\mathcal{O}^a = \sum_{\vec{u},\vec{v}} \overline{\zeta}(\vec{u})\gamma_5\frac{\tau^a}{2}\zeta(\vec{v}), \quad \mathcal{O}'^a = \sum_{\vec{u},\vec{v}} \overline{\zeta}'(\vec{u})\gamma_5\frac{\tau^a}{2}\zeta'(\vec{v}). \tag{IV.5}$$

The normalization factor

$$n_P = 1 + am + 3\left(1 - \cos\frac{a\theta}{L}\right) \tag{IV.6}$$

is chosen to give $Z_P(g_0 = 0, a/L) = 1$ at tree level on the lattice, where the quark mass am is written in terms of the PCAC mass as

$$am = -1 - 3\left(1 - \cos\frac{a\theta}{L}\right) + \sqrt{2am_{\mathrm{PCAC}} + \sqrt{1 + 4a^2m_{\mathrm{PCAC}}^2 + 6\sin^2\frac{a\theta}{L} + \left(3\sin^2\frac{a\theta}{L}\right)^2}}. \tag{IV.7}$$

The normalization factor n_P is calculated by setting $\theta = 0.5$ and the PCAC mass at each (β, κ).

The value of the renormalization factors are listed in table I at each parameter together with the step scaling function (II.3). In the table we notice that there is a tiny difference in the renormalized coupling $\overline{g}^2(L)$ between three boxes $L/a = 4, 6, 8$. We adopt the coupling at $L/a = 8$ to define the renormalization scale and the deviation is corrected perturbatively [19]. Statistics of the runs are given in table II together with values of the PCAC mass defined by

$$m_{\mathrm{PCAC}} = \frac{\frac{1}{2}\left(\nabla_0 + \nabla_0^*\right) f_A(\frac{T}{2}) + c_A \nabla_0^* \nabla_0 f_P(\frac{T}{2})}{2 f_P(\frac{T}{2})}, \tag{IV.8}$$

$$f_A(x_0) = -\frac{1}{N_f^2 - 1}\frac{a^3}{L^3}\sum_{\vec{x}}\left\langle \left(A_0^{\mathrm{imp.}}\right)^a(x)\mathcal{O}^a\right\rangle \tag{IV.9}$$

in terms of the improved axial vector current with non-perturbative improvement coefficient [20]

$$A_\mu^{\mathrm{imp.}}(x) = A_\mu(x) + c_A \partial_\mu P(x), \quad c_A(g_0^2) = -0.0038 g_0^2 \frac{1 - 0.195 g_0^2}{1 - 0.279 g_0^2}, \tag{IV.10}$$

$$A_\mu^a(x) = \overline{\psi}(x)\gamma_\mu\gamma_5\frac{1}{2}\tau^a\psi(x). \tag{IV.11}$$

B. Perturbative improvement and continuum limit

We perform a perturbative improvement of the SSF before taking the continuum limit. For this purpose we need a perturbative evaluation of the lattice artifact in the SSF

$$\delta_P(u, a/L) = \frac{\Sigma_P\left(u, a/L\right) - \sigma_P(u)}{\sigma_P(u)}. \tag{IV.12}$$

For the SSF of the running coupling the artifact $\delta(u, a/L)$ was evaluated at one loop level [13, 21]. However, the magnitude of the one-loop correction was found to be large and hence the range of applicability is limited only for very weak coupling region for our lattice action, revealing the importance of two-loop coefficient [9]. Since δ_P is not known at all for our setup, instead of calculating δ_P at one and two-loop level perturbatively we calculate SSF's directly by Monte-Carlo simulations at very weak coupling $\beta \geq 10$. The same value of κ is used as in Ref. [9], which gives almost vanishing PCAC mass there. The results are listed in table III with the number of configurations and the value of PCAC mass given in table IV.

We define $\delta_P(u, a/L)$ by the deviation from the perturbative SSF's $\sigma_P^{(2)}$ at two-loop order [19]

$$\delta_P(u, a/L) = \frac{\Sigma_P\left(u, a/L\right) - \sigma_P^{(2)}(u)}{\sigma_P^{(2)}(u)}. \tag{IV.13}$$

The deviation is fitted to a polynomial form for each a/L,

$$1 + \delta_P(u, a/L) = 1 + d_1(a/L)u + d_2(a/L)u^2. \tag{IV.14}$$

We tried a quadratic fit using data at $u \leq 1.524$, which is plotted in Fig. 1. Since the quadratic fit provides a reasonable description of data we opt to cancel the $O(a)$ contribution dividing out the SSF by the quadratic fit

$$\Sigma_P^{(2)}\left(u, \frac{a}{L}\right) = \frac{\Sigma_P\left(u, a/L\right)}{1 + d_1(a/L)u + d_2(a/L)u^2}. \tag{IV.15}$$

We notice that the deviation is consistent with zero within one standard deviation for $\delta_P(u, 1/8)$ even at $u \gtrsim 1$. We consider a large deviation in the quadratic fit is an artifact due to relatively large statistical error for the data at $u \gtrsim 1$ and we therefore do not apply the present improvement for $a/L = 1/8$. Even if we apply the improvement to the SSF $\delta_P(u, 1/8)$, the quark mass renormalization factor changes only by $\mathcal{O}(1\%)$, which is within statistical errors.

We give the values of the perturbatively improved SSF's in table V for three lattice spacings at each of the 7 renormalization scales. Scaling behavior of the improved SSF is plotted in Fig. 2. Almost no scaling violation is found. We performed three types of continuum extrapolation: a constant extrapolation with the finest two (filled symbols) or all three data points (open symbols), or a linear extrapolation with all three data points (open circles), which are consistent with each other. We employed the constant fit with the finest two data points to find our continuum value.

The RG running of the continuum SSF is plotted in Fig. 3. A polynomial fit of the continuum SSF to third order yields

$$\sigma_P(u) = 1 + p_0 u + p_1 u^2 + p_2 u^3, \tag{IV.16}$$

$$p_1 = -0.002826, \quad p_2 = 0.000031 \tag{IV.17}$$

fixing the first coefficients to its perturbative value $p_0 = -8\ln 2/(4\pi)^2$. We notice that p_1 is consistent with its perturbative value $p_1^{(\mathrm{PT})} = -0.00282843$ at two loops. The fitting function is also plotted (solid line) together with the two loops perturbative running (dashed line).

C. Non-perturbative running mass

Once $\overline{m}(1/L_{\mathrm{max}})/M$ is evaluated from the SSF given in (IV.16) according to the strategy in sect.II, we are able to derive the non-perturbative running mass in the SF scheme according to (II.6). The running mass at scale $\mu = 1/L_n$ is given in units of the RGI mass M by

$$\frac{\overline{m}(1/L_n)}{M} = w_n^{-1}\frac{\overline{m}(1/L_{\max})}{M}. \tag{IV.18}$$

The result is plotted in Fig. 4 as a function of $\mu/\Lambda_{\rm SF}$. The solid line is perturbative running given by using $\tau(g)$ at two-loop order and $\beta(g)$ at three-loop order in (II.1) with inputs of $\overline{m}(1/L_{12})M$ and $\overline{g}(1/L_{12})$ at a very high energy scale of $L_{12} = 2^{-12}L_{\max}$. We omit the horizontal error bar, which may be introduced from that of $\Lambda_{\rm SF}$.

V. Z_P AT LOW ENERGY SCALE

Some years ago CP-PACS and JLQCD Collaborations jointly performed an $N_f = 2 + 1$ simulation with the $O(a)$ improved Wilson action and the Iwasaki gauge action [10]. Three values of β, 1.83, 1.90 and 2.05 were adopted to take the continuum limit and the up-down quark mass covered a rather heavy region corresponding to $m_\pi/m_\rho = 0.63 - 0.78$. This project has been taken over by the PACS-CS Collaboration aiming at simulations at the physical light quark masses [11, 12]. At present result at a single lattice spacing $\beta = 1.90$ is available with very light quark masses down to $m_\pi/m_\rho \approx 0.2$.

One of the purpose of this paper is to provide the non-perturbative renormalization factor to renormalize the bare PCAC quark masses measured in these large scale simulations. We start by introducing a reference scale $L_{\max}$. For this purpose, the renormalized coupling is evaluated at the same bare coupling β as in the CP-PACS/JLQCD simulations and in the chiral limit [9]. The reference scale $L_{\max}$ is given by the box size we adopt in this evaluation. The renormalized coupling $\overline{g}^2(L_{\max})$ should not exceed our maximal value 5.13 for the coupling SSF significantly. We use the box size of $L/a = 4$ for $\beta = 1.83$ and 1.90 to define $L_{\max}$ and $L/a = 6$ for $\beta = 2.05$. A physical scale is introduced into the present work so that the reference scale is translated into MeV units. We employ three types of hadron masses m_π, m_ρ, m_K (m_ϕ) [10] or m_π, m_K, m_Ω [11, 12] as inputs and use the lattice spacing a as an intermediate scale, which is given in Table VI.

Then we evaluate the pseudo scalar density renormalization factor at the same $\beta = 6/g_0^2$ and κ as that in Ref. [9] to give the denominator of the PCAC mass renormalization factor (II.7). The values of the renormalized coupling constant [9] and the renormalization factor $Z_P(g_0, a/L_{\max})$ are listed in Table VII.

VI. AXIAL CURRENT RENORMALIZATION FACTOR

The remaining ingredient of the renormalization factor (II.7) at low energy is that of the axial vector current. We calculate the renormalization factor according to the procedure in Ref. [22, 23] through the axial Ward-Takahashi identity. We adopt the renormalization condition [23]

$$Z_A^2(g_0, m) = \widetilde{Z}_A\left(g_0, m, \frac{3}{2}T\right), \tag{VI.1}$$

$$\widetilde{Z}_A\left(g_0, m, x_0\right) = \frac{1}{n_A}\frac{f_1}{f_{AA}^I\left(x_0, \frac{1}{3}T\right) - 2m_{\rm PCAC}\widetilde{f}_{PA}^I\left(x_0, \frac{1}{3}T\right)}, \tag{VI.2}$$

which is applicable to small non-vanishing PCAC mass. In this section we suppress the a/L_{max} dependence while we explicitly write the m dependence instead. Here f_{AA}^I and $\widetilde{f}_{PA}^I$ are four-point functions of boundary operators and the improved axial current (IV.10) or the pseudo scalar density operator (IV.4) defined by

$$f_{AA}^I(x_0, y_0) = -\frac{1}{6L^6}\sum_{\vec{x}\vec{y}} \epsilon^{abc}\epsilon^{cde}\left\langle \mathcal{O}'^d \left(A_0^{\text{imp.}}\right)^a(x)\left(A_0^{\text{imp.}}\right)^b(y)\mathcal{O}^e\right\rangle, \tag{VI.3}$$

$$\widetilde{f}_{PA}^I(x_0, y_0) = -\frac{1}{6L^6}\sum_{\vec{x}\vec{y}} \epsilon^{abc}\epsilon^{cde}\left\langle \mathcal{O}'^d P^a(x)\left(A_0^{\text{imp.}}\right)^b(y)\mathcal{O}^e\right\rangle. \tag{VI.4}$$

The PCAC mass here is given by an average over three time slices

$$m_{\text{PCAC}} = \frac{1}{3}\sum_{x_0=\frac{T}{2}-1}^{\frac{T}{2}+1} \frac{\frac{1}{2}\left(\nabla_0 + \nabla_0^*\right) f_A(x_0) + c_A \nabla_0^*\nabla_0 f_P(x_0)}{2 f_P(x_0)}. \tag{VI.5}$$

The normalization factor n_A is chosen to give $\widetilde{Z}_A(g_0 = 0, m, x_0) = 1$ at tree level on the lattice.

As a byproduct we are able to derive the renormalization factor for the vector current

$$V_\mu(x) = \overline{\psi}(x)\gamma_\mu \frac{1}{2}\tau^a \psi(x) \tag{VI.6}$$

with negligible computational cost. Here again we adopt the same definition for the renormalization factor as in [22, 23] given by

$$Z_V(g_0) = \widetilde{Z}_V\left(g_0, \frac{T}{2}\right), \tag{VI.7}$$

$$\widetilde{Z}_V\left(g_0, x_0\right) = \frac{1}{n_V}\frac{f_1}{f_V(x_0)}, \tag{VI.8}$$

$$f_V(x_0) = \frac{1}{6L^6}\sum_{\vec{x}} i\epsilon^{dce}\left\langle \mathcal{O}'^d V_\mu^c(x)\mathcal{O}^e\right\rangle. \tag{VI.9}$$

The normalization factor is given by $n_V = n_P$.

There are several alternative choices in the calculation of Z_A: box size L/a, twisting angle θ and two definitions of Z_A in Ref. [22, 23] with or without the disconnected diagrams. Our requirement is that the $\mathcal{O}(a^2)$ lattice artifact is suppressed as much as possible within a reasonable computational cost. As a measure of the lattice artifact, we use the time dependence of $\widetilde{Z}_{A/V}$, which should disappear in the continuum limit.

We have varied the spatial box size from $L/a = 6$ to 12 until we find a plateau in $\widetilde{Z}_{A/V}$ as a function of x_0. Our box sizes are $6^3 \times 18$, $8^3 \times 18$, $10^3 \times 24$ and $12^3 \times 30$. The temporal lattice size was taken to be a multiple of six so that it is even and the two axial currents can be placed at an equal distance $T/(3a)$ from the boundary and from each other. We set T/a to the nearest value to $9/4 \times L/a$ [23]. The spatial twist angle is set to $\theta = 0$ and 0.5 to examine its dependence. The bare quark mass is tuned so that $|am_{\text{PCAC}}| < 0.01$ since the dependence is known to be negligible [23] in the definition (VI.2) for such a small mass. The Dirichlet boundary condition (III.1) is the same as that for Z_P.

The time dependence of $\widetilde{Z}_A(g_0, m, x_0)$ is plotted for $\beta = 1.83$ in Figs. 5 ($\theta = 0.5$) and 6 ($\theta = 0$). We found no plateau for both definitions with or without the disconnected diagram for almost all box sizes. The variation of θ does not change the conclusion. An exception is that with the disconnected diagram on a $12^3 \times 30$ lattice indicated by red diamonds. However we cannot be very confident of a plateau for two reasons. One is that the statistical error is too large and the other is a large discrepancy between the two definitions with or without the disconnected diagrams, which should be a pure lattice artifact at the massless point.

The time dependence is more tamed at $\beta = 1.90$ as is seen in Figs. 7 and 8. We found a plateau in $\widetilde{Z}_A$ with the disconnected diagram for $L/a \geq 10$ at $\theta = 0.5$ or $L/a \geq 8$ with $\theta = 0$. The value of Z_A is consistent with each other at $x_0 = 2T/3$ within one standard deviation once a plateau is located. We have no trouble to find a plateau for $\beta \geq 2.05$ as is shown in Figs. 9, 10. Furthermore results from the two definitions with or without the disconnected diagrams are consistent with each other.

We conclude that we should adopt the definition with the disconnected diagrams [23] to locate a plateau at smaller β. It is better to set the twist angle θ to zero although computational cost is slightly heavier and statistical fluctuation becomes worse. The box size should be taken as large as possible since lattice artifacts should manifest as a polynomial of a/L.

In this paper we adopted the following box size at each β to define Z_A: $12^3 \times 30$, $\theta = 0.5$ at $\beta = 1.83$, $10^3 \times 24$, $\theta = 0$ at $\beta = 1.90$ and $12^3 \times 30$, $\theta = 0.5$ for $\beta = 2.05$. The disconnected contribution is included. The physical box size varies from 0.84 fm to 1.3 fm. We derive our Z_A by fitting the plateau around $x_0 = 2T/3$ by a constant. The fitting range is plotted in Figs. 5 - 10. The error is estimated by the Jackknife method. The results are listed in tables VIII, IX and X together with those at various box sizes.

In Fig. 11 we plot the values for Z_A according to our definition (filled circles), together with those of other definitions (open symbols). Scattering of points starting around $\beta = 1.95$ indicates that lattice artifacts are increasingly large in our data for large lattice spacings.

The time dependence of $\widetilde{Z}_V(g_0, x_0)$ is plotted for $\beta = 1.83$ in Fig. 12 for $\theta = 0.5$ (left) and $\theta = 0$ (right) with horizontal axis normalized to unity. For $L/a \geq 10$ we find a long plateau whose values does not depend on L and θ. The behavior is almost the same for $\beta = 1.90$ (Fig. 13) and $\beta = 2.05$ (Fig. 14). $\widetilde{Z}_V(g_0, x_0)$ seems to be almost flat at $\beta \geq 3.0$ for $L/a = 8$ as is seen in Fig. 15. The renormalization factor Z_V given by fitting the plateau is listed in tables VIII, IX and X.

In Fig. 16 we plot our final results for $Z_A(g_0)$ and $Z_V(g_0)$ as a function of β together with perturbative behavior (solid line) and results from the tadpole improved perturbation theory (star symbols).

VII. RGI MASS RENORMALIZATION FACTOR

We derive the renormalization factor Z_M for the RGI mass according to the procedure given in Sec. II. This factor is intended to renormalize the bare PCAC masses obtained in the two large scale simulations carried out at three values of β. The three hadron masses, m_π, m_K, m_Ω were used in Ref. [11, 12] to determine the light quark masses and the lattice spacing. Two choices m_π, m_ρ m_K or m_π, m_ρ m_ϕ were adopted in Ref. [10]. The results for Z_M are listed in Table XI. Also listed are the mass renormalization factors $Z_m^{\overline{\mathrm{MS}}}(\beta, \mu = 2~\mathrm{GeV})$ in the $\overline{\mathrm{MS}}$ scheme at a renormalization scale $\mu = 2$ GeV. We emphasize that the renormalization factor here is defined in terms of the renormalization group functions for three flavors. Results from tadpole improved perturbation theory is also listed for comparison.

The error in the renormalization factor includes all the statistical and systematic ones except for that from the choice of the reference scale $L_{\rm max}$. Lattice artifacts may be present at order $\mathcal{O}((a/L_{\rm max})^2)$. In order to estimate this effect we increase $L_{\rm max}/a$ at each β. There is a problem that values of the renormalized coupling $u_{\rm max}$ and the renormalization factor $Z_P(L_{\rm max})$ tend to exceed the region covered by our step scaling function as is shown in Table XII. Since we attempt just a rough estimate, we adopted the step scaling function by extrapolating its polynomial form. The result is listed in Table XIII and by comparing with values in Table XI we find a few percent effect at $\beta = 2.05$, while the magnitude may increase to a 10 % level at lower values of β.

As the last step we apply our renormalization factor to the bare PCAC masses in Refs. [10–12] to obtain values for the renormalized quark masses. The numerical results are given in Table XIV and are plotted in Fig. 17 both for the averaged up and down quark mass (left panel) and for the strange quark mass (right panel). For the old CP-PACS/JLQCD work of Ref. [10] results with K and ϕ meson input are plotted (filled squares and triangles) together with perturbatively renormalized masses using tadpole improved renormalization factor (open squares and circles). The triangle represents the result for the more recent work of PACS-CS with the pion mass reaching down to $m_\pi = 155$ MeV.

It is disappointing that the old CP-PACS/JLQCD results do not exhibit a better scaling behavior by going from perturbative to non-perturbative renormalization factor. However, we should note a significant change in the average up and down quark mass with the recent PACS-CS work (filled triangle). This represents a systematic error due to chiral extrapolation of the old CP-PACS/JLQCD work whose pion mass reached only $m_\pi \sim 500$ MeV. We should also note that the renormalization factor Z_A involves a large uncertainty at $\beta = 1.83$ which is not reflected in the error bar of Fig. 17. We feel that results at $\beta = 2.05$ using simulation with physical pion mass are needed to find the convincing values for light quark masses with our approach.

VIII. CONCLUSION

We have presented a calculation of the quark mass renormalization factor for the $N_f = 2+1$ QCD in the mass independent Schrödinger functional scheme in the chiral limit. We adopt seven renormalization scales to cover from low to high energy region. Three lattice spacings are used to take the continuum limit. We calculate the pseudo scalar density renormalization factor and obtain the SSF for the running mass. Applying a perturbative improvement, we find that the step scaling function shows a good scaling behavior and the continuum limit may be taken safely with a constant extrapolation of the results for the finest two lattice spacings. The non-perturbative SSF turned out to be almost consistent with the perturbative two loops result.

With the non-perturbative renormalization group flow we are able to estimate the quark mass renormalization factor which renormalizes the bare PCAC mass and give the RGI mass. For this purpose we derive the renormalization factor of the pseudo scalar density at low energy and that of axial vector current. The results are used to renormalized the PCAC masses in the two recent large scale simulations [10–12]. We also evaluate the non-perturbative factor $Z_m^{\overline{\rm MS}}(\beta, \mu = 2~{\rm GeV})$ in $\overline{\rm MS}$ scheme at a scale $\mu = 2$ GeV.

All statistical and systematic errors are included in the renormalization factor Z_M except for that due to the choice of the reference scale $L_{\rm max}$. A rough estimate of $\mathcal{O}((a/L_{\rm max})^2)$ effect suggests possible 10 % systematic error at $\beta = 1.90$. However, a firmer conclusion requires the step scaling function at the couplings stronger than those explored in the present work. We leave it as future work to examine this issue.

Applying our non-perturbative renormalization factor to the present PACS-CS simulation with the pion mass as light as $m_\pi = 155$ MeV yields $m_{ud}^{\overline{\rm MS}}(\mu = 2~{\rm GeV}) = 2.78(27)$ MeV for the average up and down quark, and $m_s^{\overline{\rm MS}}(\mu = 2~{\rm GeV}) = 86.7(2.3)$ MeV for the strange quark. Simulations at weaker couplings under way will tell if these values stay toward the continuum limit.

Acknowledgments

This work is supported in part by Grants-in-Aid of the Ministry of Education, Culture, Sports, Science and Technology-Japan (Nos. 18104005, 20105001, 20105002, 20105003, 20105005, 20340047, 20540248, 21340049, 22105501, 22244018, 22740138). Part of the calculations were performed by using the RIKEN Integrated Cluster of Clusters facilities.

---

[1] M. Lüscher, R. Narayanan, P. Weisz and U. Wolff, Nucl. Phys. B **384** (1992) 168. [arXiv:hep-lat/9207009].

[2] M. Lüscher, R. Sommer, P. Weisz and U. Wolff, Nucl. Phys. B **413** (1994) 481. [arXiv:hep-lat/9309005].

[3] S. Sint, Nucl. Phys. B **421** (1994) 135 [arXiv:hep-lat/9312079].

[4] M. Lüscher, S. Sint, R. Sommer and P. Weisz "Chiral symmetry and O(a) improvement in lattice QCD," Nucl. Phys. B **478** (1996) 365 [arXiv:hep-lat/9605038].

[5] S. Capitani, M. Lüscher, R. Sommer and H. Wittig [ALPHA Collaboration], Nucl. Phys. B **544** (1999) 669. [arXiv:hep-lat/9810063].

[6] S. Sint, Nucl. Phys. Proc. Suppl. **94** (2001) 79 [arXiv:hep-lat/0011081] and references there in.

[7] M. Della Morte, R. Frezzotti, J. Heitger, J. Rolf, R. Sommer and U. Wolff [ALPHA Collaboration], Nucl. Phys. B **713** (2005) 378. [arXiv:hep-lat/0411025].

[8] M. Della Morte, R. Hoffmann, F. Knechtli, J. Rolf, R. Sommer, I. Wetzorke and U. Wolff [ALPHA Collaboration], Nucl. Phys. B **729** (2005) 117. [arXiv:hep-lat/0507035].

[9] S. Aoki *et al.* [PACS-CS Collaboration], JHEP **10** (2009) 053. [arXiv:0906.3906 [hep-lat]].

[10] T. Ishikawa *et al.* [JLQCD Collaboration], Phys. Rev. D **78** (2008) 011502. [arXiv:0704.1937 [hep-lat]].

[11] S. Aoki *et al.* [PACS-CS Collaboration], Phys. Rev. D **79** (2009) 034503. [arXiv:0807.1661 [hep-lat]].

[12] Y. Kuramashi [PACS-CS Collaboration], PoS LATTICE2009;???, 2009

[13] S. Takeda, S. Aoki and K. Ide, Phys. Rev. D **68** (2003) 014505. [arXiv:hep-lat/0304013].

[14] S. Aoki *et al.* [CP-PACS Collaboration], Phys. Rev. D **73** (2006) 034501. [arXiv:hep-lat/0508031].

[15] S. Aoki, R. Frezzotti and P. Weisz, Nucl. Phys. B **540** (1999) 501. [arXiv:hep-lat/9808007].

[16] S. Sint and P. Weisz [ALPHA collaboration], Nucl. Phys. B **545** (1999) 529 [arXiv:hep-lat/9808013].

[17] `http://qcdoc.phys.columbia.edu/cps.html`

[18] `http://www.open-supercomputer.org/index.html`

[19] A. Bode, P. Weisz and U. Wolff [ALPHA collaboration], Nucl. Phys. B **576** (2000) 517 [Erratum-ibid. B **600** (2001 ERRATA,B608,481.2001) 453]. [arXiv:hep-lat/9911018].

[20] T. Kaneko, S. Aoki, M. Della Morte, S. Hashimoto, R. Hoffmann and R. Sommer, JHEP **0704** (2007) 092. [arXiv:hep-lat/0703006].

[21] S. Takeda, Private communication.

[22] M. Lüscher, S. Sint, R. Sommer and H. Wittig, Nucl. Phys. B **491** (1997) 344. [arXiv:hep-lat/9611015].

[23] M. Della Morte, R. Hoffmann, F. Knechtli, R. Sommer and U. Wolff, JHEP **0507** (2005) 007. [arXiv:hep-lat/0505026].

β	κ	L/a	$u = \overline{g}^2(L)$	$Z_P(g_0, L/a)$	$2L/a$	$Z_P(g_0, 2L/a)$	$\Sigma_P(u, a/L)$
2.15747	0.134249	4	3.4102(99)	0.68631(56)	8	0.5559(10)	0.8095(17)
2.34652	0.134439	6	3.415(16)	0.64909(91)	12	0.5464(22)	0.8416(36)
2.5	0.133896	8	3.418(19)	0.64138(86)	16	0.5469(19)	0.8527(34)
2.5352	0.132914	4	2.6299(29)	0.75417(51)	8	0.64852(95)	0.8598(14)
2.73466	0.133083	6	2.6292(77)	0.71639(68)	12	0.6349(14)	0.8862(22)
2.9	0.132658	8	2.6317(125)	0.70575(63)	16	0.6312(18)	0.8944(28)
2.9605	0.131831	4	2.1279(23)	0.80163(44)	8	0.71330(87)	0.8898(12)
3.16842	0.131997	6	2.1249(56)	0.76386(50)	12	0.69554(73)	0.9104(12)
3.3	0.131743	8	2.1289(92)	0.74887(68)	16	0.6808(14)	0.9091(21)
3.33886	0.131092	4	1.8426(19)	0.82973(38)	8	0.75240(85)	0.9069(11)
3.55351	0.131244	6	1.8375(32)	0.79389(42)	12	0.73496(68)	0.9256(10)
3.7	0.131021	8	1.8403(59)	0.77923(55)	16	0.7224(12)	0.9271(17)
3.93653	0.130195	4	1.5248(10)	0.86074(35)	8	0.79485(72)	0.92348(92)
4.15042	0.130356	6	1.5300(40)	0.82826(38)	12	0.77829(57)	0.93955(81)
4.3	0.1302	8	1.5242(35)	0.81401(47)	16	0.7652(11)	0.9400(15)
4.74	0.12934	4	1.24874(84)	0.88808(28)	8	0.83339(62)	0.93842(76)
4.94755	0.129495	6	1.2483(15)	0.85871(34)	12	0.81476(41)	0.94880(61)
5.1	0.129376	8	1.2488(28)	0.84501(40)	16	0.80536(82)	0.9531(11)
5.87312	0.128517	4	0.99982(61)	0.91197(27)	8	0.86779(48)	0.95152(60)
6.06879	0.12867	6	1.00130(97)	0.88669(29)	12	0.85142(41)	0.96026(56)
6.2	0.1286	8	1.0006(16)	0.87496(24)	16	0.84102(70)	0.96121(84)

TABLE I: The pseudo scalar density renormalization factor Z_P at scale L and $2L$. The value of β and κ has been tuned to reproduce the same physical box size L and near zero PCAC mass in Ref. [9]. The step scaling function Σ_P is also listed.

β	κ	L/a	# of confs.	$m_{\rm PCAC}$	$2L/a$	# of confs.	$m_{\rm PCAC}$
2.15747	0.134249	4	19600	0.03103(24)	8	12600	0.03876(13)
2.34652	0.134439	6	10300	0.00264(18)	12	7600	0.002856(78)
2.5	0.133896	8	15200	0.000753(79)	16	9800	0.000517(35)
2.5352	0.132914	4	20000	0.02587(19)	8	8000	0.02808(11)
2.73466	0.133083	6	12000	0.00251(10)	12	8200	0.001792(55)
2.9	0.132658	8	24000	0.000781(47)	16	8300	0.000502(27)
2.9605	0.131831	4	20000	0.02179(15)	8	8000	0.021887(62)
3.16842	0.131997	6	22000	0.001917(74)	12	26800	0.001093(20)
3.3	0.131743	8	16000	0.000479(49)	16	13200	0.000280(17)
3.33886	0.131092	4	20000	0.01937(12)	8	8000	0.018782(68)
3.55351	0.131244	6	20800	0.002015(60)	12	24300	0.001005(18)
3.7	0.131021	8	16000	0.000492(38)	16	12200	0.000231(16)
3.93653	0.130195	4	20000	0.016138(93)	8	8000	0.015220(45)
4.15042	0.130356	6	16000	0.001450(47)	12	23600	0.000604(13)
4.3	0.1302	8	16000	−0.000088(31)	16	10200	−0.000260(14)
4.74	0.12934	4	20000	0.013028(79)	8	8000	0.011884(41)
4.94755	0.129495	6	16000	0.001371(41)	12	35200	0.0005863(92)
5.1	0.129376	8	16000	0.000243(25)	16	14100	0.0000853(89)
5.87312	0.128517	4	20000	0.010385(62)	8	8000	0.009065(33)
6.06879	0.12867	6	16000	0.000910(31)	12	19200	0.0002673(99)
6.2	0.1286	8	32000	0.000103(14)	16	11000	−0.0000139(89)

TABLE II: Number of configurations for each run. Also listed is the PCAC mass at each parameter.

β	κ	L/a	$u = \bar{g}^2(L)$	$Z_P(g_0, L/a)$	$2L/a$	$Z_P(g_0, 2L/a)$	$\Sigma_P(u, a/L)$
10	0.1270893	4	0.58565(34)	0.95007(21)	8	0.92391(27)	0.97247(36)
20	0.1260654	4	0.29543(17)	0.975596(93)	8	0.96211(11)	0.98618(15)
40	0.1255571	4	0.14876(23)	0.987683(80)	8	0.981223(64)	0.99346(10)
60	0.1253871	4	0.099336(40)	0.991832(46)	8	0.9873514(42)	0.995482(62)
10	0.1272305	6	0.59707(44)	0.93262(13)	12	0.91141(31)	0.97726(36)
20	0.1261216	6	0.29775(33)	0.96681(11)	12	0.95557(13)	0.98837(18)
40	0.1255700	6	0.149219(45)	0.983422(56)	12	0.977882(57)	0.994366(81)
60	0.1253863	6	0.099664(47)	0.988962(38)	12	0.985302(42)	0.996299(57)
10	0.1272310	8	0.6051(12)	0.92377(19)	16	0.90192(77)	0.97635(85)
20	0.1261176	8	0.29971(49)	0.962064(82)	16	0.95088(29)	0.98837(31)
40	0.1255626	8	0.14948(27)	0.981092(50)	16	0.97552(10)	0.99432(12)

TABLE III: The pseudo scalar density renormalization factor Z_P at scale L and $2L$ at very weak coupling region $\beta \geq 10$. The step scaling function Σ_P is also listed.

β	κ	L/a	# of confs.	$m_{\rm PCAC}$	$2L/a$	# of confs.	$m_{\rm PCAC}$
10	0.1270893	4	9700	0.005287(49)	8	7200	0.004447(20)
20	0.1260654	4	10000	0.002057(23)	8	7200	0.001461(8)
40	0.1255571	4	10000	0.000401(14)	8	7200	−0.000084(4)
60	0.1253871	4	10000	−0.000128(8)	8	7200	−0.000558(3)
10	0.1272305	6	20000	0.000296(17)	12	8000	−0.0001431(94)
20	0.1261216	6	10000	−0.000122(12)	12	7200	−0.0004012(50)
40	0.1255700	6	10000	−0.000353(6)	12	7200	−0.0005258(26)
60	0.1253863	6	10000	−0.000417(4)	12	7200	−0.0005604(15)
10	0.1272310	8	12000	−0.000069(14)	16	3600	−0.0001635(93)
20	0.1261176	8	12000	−0.000216(7)	16	2700	−0.0002723(67)
40	0.1255626	8	14400	−0.000256(3)	16	2700	−0.0002934(24)

TABLE IV: Number of configurations for each run at very weak coupling. Also listed is the PCAC mass at each parameter.

u	$\sigma_P(u)$	$\Sigma_P(u,1/8)$	$\Sigma_P^{(2)}(u,1/6)$	$\Sigma_P^{(2)}(u,1/4)$
1.0006	0.96165(47)	0.96121(84)	0.96185(56)	0.96206(60)
1.2488	0.95117(53)	0.9531(11)	0.95055(61)	0.95177(77)
1.5242	0.94113(74)	0.9400(15)	0.94136(82)	0.94002(94)
1.8403	0.92730(86)	0.9271(17)	0.9274(10)	0.9272(11)
2.1289	0.9113(10)	0.9091(21)	0.9119(12)	0.9136(12)
2.6317	0.8898(17)	0.8944(28)	0.8872(22)	0.8898(14)
3.4178	0.8474(25)	0.8527(34)	0.8411(36)	0.8493(18)

TABLE V: The perturbatively improved SSF $\Sigma_P^{(2)}(u,a/L)$ at "two loop" level. The improvement is not applied for $a/L=1/8$. The SSF $\sigma_P(u)$ in the continuum is also listed, which is given by a constant fit of two data at finest lattice spacings 1/6, 1/8.

β	K-input[10]	ϕ-input[10]	K-input[12]
1.83	0.1174(23)	0.1184(26)	0.08995(40)
1.90	0.0970(26)	0.0971(25)	
2.05	0.0701(29)	0.0702(28)	

TABLE VI: Lattice spacing a in unit of fm from large scale simulations [10] and [11, 12].

β	κ	$L_{\max}/a$	$\overline{g}^2(L_{\max})$	$Z_P(g_0, a/L_{\max})$
1.83	0.13608455	4	5.565(54)	0.57519(32)
1.90	0.1355968	4	4.695(23)	0.60784(27)
2.05	0.1359925	6	4.740(79)	0.56641(44)

TABLE VII: The renormalized coupling and the renormalization factor Z_P at $\beta = 1.83$, 1.90, 2.05 for low energy scale $L_{\max}$.

	size	β	κ	θ	traj.	$m_{\rm PCAC}$	Z_V	Z_A	$Z_A^{\rm con}$
	$6^3 \times 18$	1.83	0.138466	0.5	149000	−0.00065(67)	0.7533(16)	0.553(25)	0.9622(88)
	$6^3 \times 18$	1.83	0.138466	0	22300	0.0083(28)	0.7390(16)	0.84(33)	0.938(18)
	$8^3 \times 18$	1.83	0.138616	0.5	128000	−0.00036(52)	0.71343(32)	0.650(10)	0.9317(90)
	$8^3 \times 18$	1.83	0.138616	0	19200	0.00081(97)	0.71522(71)	0.626(15)	0.947(13)
	$10^3 \times 24$	1.83	0.138640	0.5	5400	0.0037(17)	0.7022(11)	0.609(45)	0.927(49)
	$10^3 \times 24$	1.83	0.138640	0	8800	0.0009(10)	0.70768(66)	0.594(24)	0.963(23)
$*$	$12^3 \times 30$	1.83	0.138700	0.5	3700	−0.0006(23)	0.7013(14)	0.619(70)	0.95(17)

TABLE VIII: The (axial) vector current renormalization factor at $\beta = 1.83$ for various box sizes. Two choices of $\theta = 0.5$ and $\theta = 0$ are adopted for comparison. We also listed Z_A without disconnected diagrams as $Z_A^{\rm con}$. Data with star symbol is adopted for our Z_A.

	size	β	κ	θ	traj.	$m_{\rm PCAC}$	Z_V	Z_A	$Z_A^{\rm con}$
	$8^3 \times 18$	1.90	0.137556	0.5	88700	0.00129(36)	0.74157(64)	0.729(15)	0.8526(48)
	$8^3 \times 18$	1.90	0.137600	0	128000	−0.00042(28)	0.74365(44)	0.7578(69)	0.8529(88)
	$10^3 \times 24$	1.90	0.137556	0.5	11300	0.00256(66)	0.73321(49)	0.716(24)	0.873(15)
$*$	$10^3 \times 24$	1.90	0.137556	0	40800	0.00191(41)	0.7354(37)	0.781(20)	0.874(13)
	$12^3 \times 30$	1.90	0.137503	0.5	4000	0.00664(81)	0.73048(66)	0.728(70)	0.850(85)

TABLE IX: The (axial) vector current renormalization factor at $\beta = 1.90$ for various box sizes. Two choices of $\theta = 0.5$ and $\theta = 0$ are adopted for comparison. We also listed Z_A without disconnected diagrams as $Z_A^{\rm con}$. Data with star symbol is adopted for our Z_A.

	size	β	κ	traj.	$m_{\rm PCAC}$	Z_V	Z_A	$Z_A^{\rm con}$
	$8^3 \times 18$	2.05	0.136116	14400	0.00305(40)	0.78369(99)	0.8145(52)	0.8211(22)
$*$	$12^3 \times 30$	2.05	0.136116	5400	0.00201(29)	0.77314(82)	0.804(15)	0.8119(28)
$*$	$8^3 \times 18$	3.0	0.132420	7200	0.00070(14)	0.87109(91)	0.88578(57)	0.88335(95)
$*$	$8^3 \times 18$	4.0	0.130581	8100	−0.000032(58)	0.90495(82)	0.91405(83)	0.91420(74)
$*$	$8^3 \times 18$	5.0	0.129471	5500	−0.000060(66)	0.9245(13)	0.93183(39)	0.93154(31)

TABLE X: The (axial) vector current renormalization factor at $\beta = 2.05$ and larger for $\theta = 0.5$. We also listed Z_A without disconnected diagrams as $Z_A^{\rm con}$. Data with star symbol is adopted for our Z_A.

β	Z_M	$Z_m^{\overline{\mathrm{MS}}}$ (K)	PT(tad) $Z_m^{\overline{\mathrm{MS}}}$ (K)	$Z_m^{\overline{\mathrm{MS}}}$ (ϕ)	PT(tad) $Z_m^{\overline{\mathrm{MS}}}$ (ϕ)
1.83 [10]	1.33(15)	1.04(12)	1.07161	1.04(12)	1.07019
1.90 [10]	1.693(46)	1.315(35)	1.09973	1.315(35)	1.09955
2.05 [10]	1.862(41)	1.417(29)	1.14487	1.416(29)	1.1446
1.90 [12]	1.693(46)	1.347(36)	1.11322		

TABLE XI: Z_M for the RGI mass and $Z_m^{\overline{\mathrm{MS}}}(2 \text{ GeV})$ in the $\overline{\mathrm{MS}}$ scheme, which are designed to renormalize the bare PCAC mass in two recent simulations of Ref. [10] and [11, 12]. (K) or (ϕ) means which meson mass is used for physical scale input. Perturbative results with tadpole improvement are also listed for $Z_m^{\overline{\mathrm{MS}}}(2 \text{ GeV})$. A slight difference in $Z_m^{\overline{\mathrm{MS}}}$ at $\beta = 1.90$ between Ref. [10] and [12] is due to that of the lattice spacing, from which physical unit is introduced.

β	κ	$L_{\max}/a$	$\overline{g}^2$	m_{PCAC}	Z_P	m_{PCAC}
1.83	0.138192	6	9.37(27)	0.00231(59)	0.44601(86)	0.00439(35)
1.90	0.137289	6	6.60(12)	0.00035(37)	0.49605(66)	0.00313(22)
2.05	0.13611599	8	6.01(21)	0.00026(15)	0.51155(57)	0.000733(74)

TABLE XII: The renormalized coupling $\overline{g}^2$ and the renormalization factor Z_P at larger box size of $L_{\max}/a$ at three β's. Two PCAC masses are evaluated with different Dirichlet boundary condition.

β	Z_M	$Z_m^{\overline{\mathrm{MS}}}$ (K)
1.83 [10]	1.46(18)	1.15(14)
1.90 [10]	1.837(57)	1.418(41)
2.05 [10]	1.890(47)	1.437(31)
1.90 [12]	1.837(57)	1.452(42)

TABLE XIII: Z_M and $Z_m^{\overline{\mathrm{MS}}}(2 \text{ GeV})$ evaluated with larger box size $L_{\max}$.

β	M_{ud}^{RGI} (K)	$m_{ud}^{\overline{\mathrm{MS}}}$ (K)	M_s^{RGI} (K)	$m_s^{\overline{\mathrm{MS}}}$ (K)	M_{ud}^{RGI} (ϕ)	$m_{ud}^{\overline{\mathrm{MS}}}$ (ϕ)	M_s^{RGI} (ϕ)	$m_s^{\overline{\mathrm{MS}}}$ (ϕ)
1.83 [10]	3.30(38)	2.59(30)	86(10)	67.7(7.9)	3.31(39)	2.58(30)	99(11)	77.7(9.0)
1.90 [10]	4.47(17)	3.47(13)	115.3(4.4)	89.5(3.4)	4.46(16)	3.46(12)	124.8(5.4)	96.9(4.2)
2.05 [10]	5.29(24)	4.02(18)	136.1(6.5)	103.6(4.9)	5.29(24)	4.02(18)	143.0(8.1)	108.8(6.1)
1.90 [12]	3.49(34)	2.78(27)	109.0(3.0)	86.7(2.3)				

TABLE XIV: Non-perturbatively renormalized mass for the averaged up and down quark and for the strange quark in the two recent simulations of Ref. [10–12]. M^{RGI} is the RGI mass and $m^{\overline{\mathrm{MS}}}$ is that in the $\overline{\mathrm{MS}}$ scheme at a scale $\mu = 2$ GeV. The unit is in MeV. (K) or (ϕ) means which meson mass is used for physical scale input.

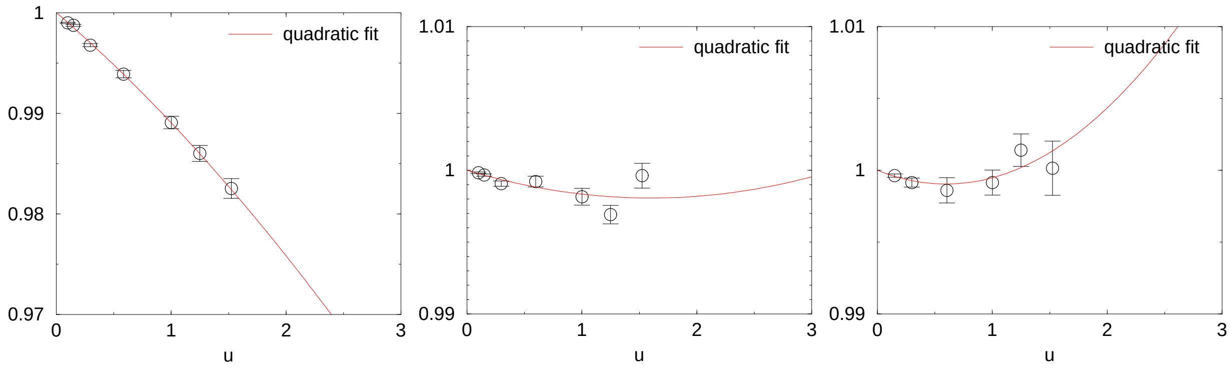

FIG. 1: The polynomial fit of the discrepancy $\Sigma_P\left(u, a/L\right)/\sigma_P^{(2)}(u)$ at high $\beta \gtrsim 4$. The fit is given for each lattice spacings $a/L = 1/4$ (left), 1/6 (middle) and 1/8 (right). Solid line is a quadratic fit.

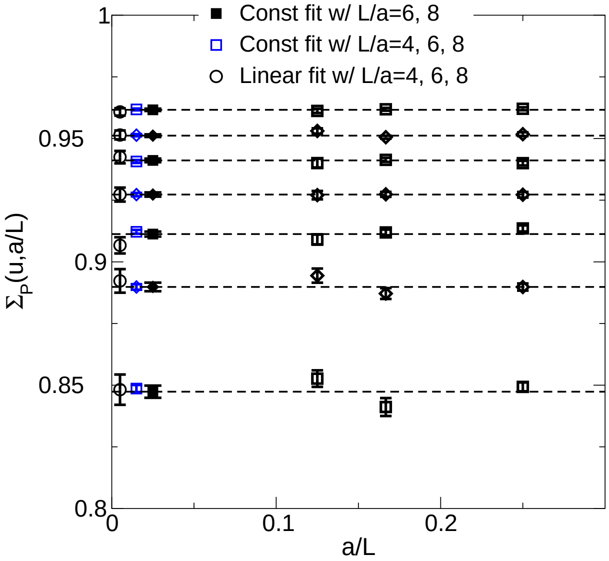

FIG. 2: The SSF on the lattice with its continuum extrapolation at each renormalization scale. Three types of continuum extrapolation are tried: a constant extrapolation with the finest two (filled symbols) or all three data points (open symbols), or a linear extrapolation with all three data points (open circles). These are consistent with each other.

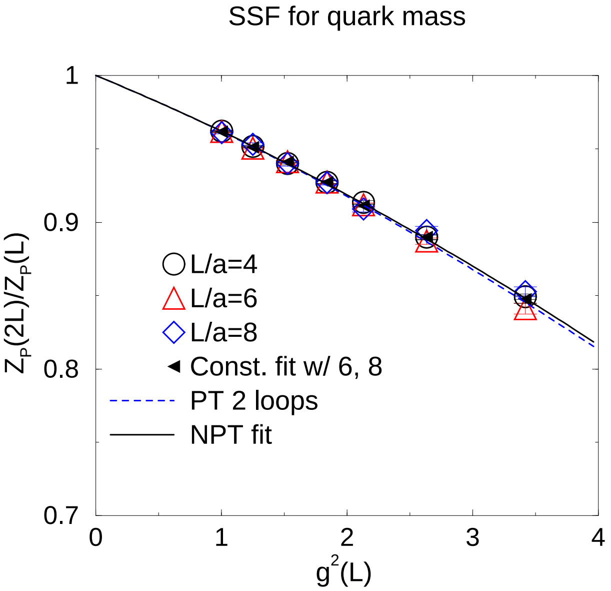

FIG. 3: The RG flow of the SSF. Dotted line is two loops perturbative running. Solid line is a polynomial fit of the SSF.

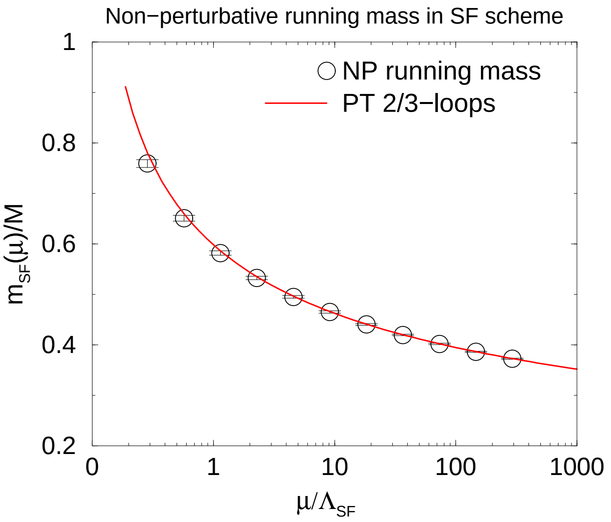

FIG. 4: The non-perturbative running mass in the SF scheme. Solid line is a perturbative running with two and three loops RG function for the mass and the coupling.

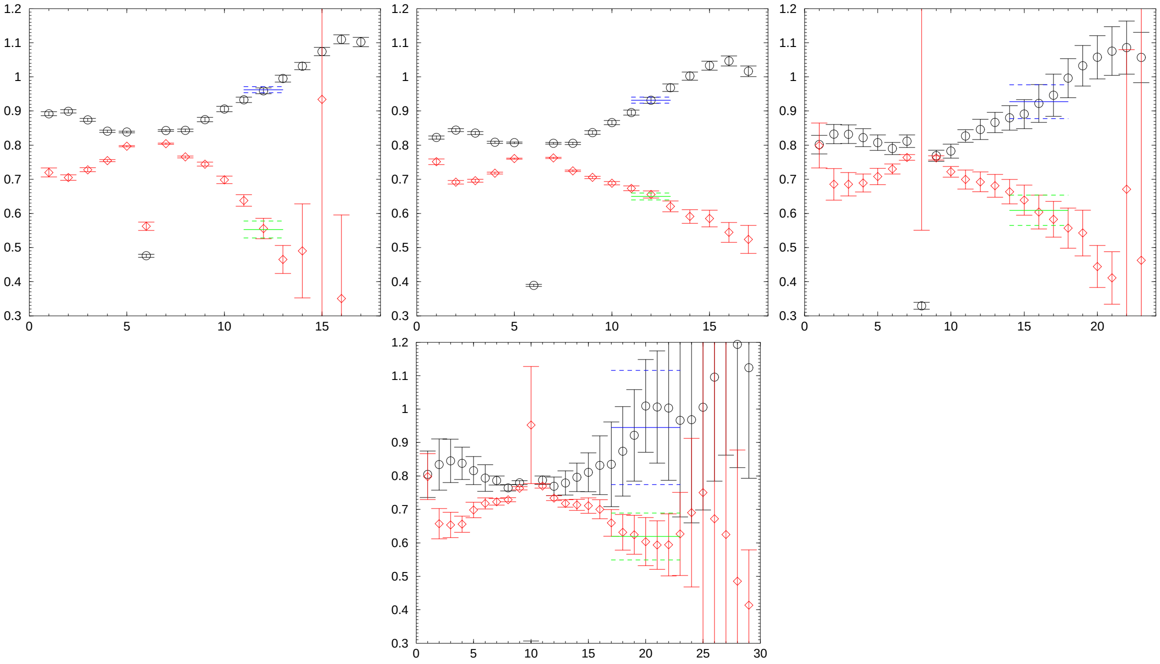

FIG. 5: x_0 dependence of $\widetilde{Z}_A(g_0, m, x_0)$ at $\beta = 1.83$ and $\theta = 0.5$ for box sizes $6^3 \times 18$ (upper left), $8^3 \times 18$ (upper middle), $10^3 \times 24$ (upper right) and $12^3 \times 30$ (lower). Red diamonds and black circles are definition with or without the disconnected diagrams. Solid and dashed lines represent an expected plateau, which is given by fitting data around $x_0 = 2T/3$ by a constant. Error is estimated with the Jackknife method.

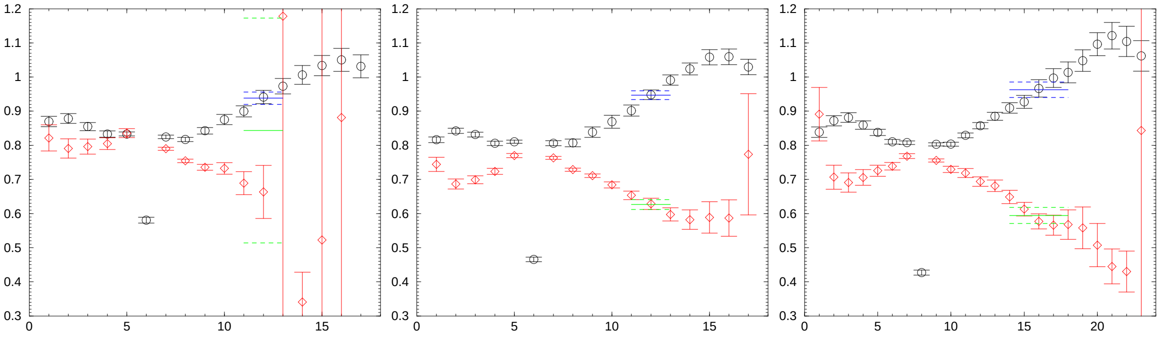

FIG. 6: x_0 dependence of $\widetilde{Z}_A(g_0, m, x_0)$ at $\beta = 1.83$ and $\theta = 0$ for box sizes $6^3 \times 18$ (left), $8^3 \times 18$ (middle) and $10^3 \times 24$ (right).

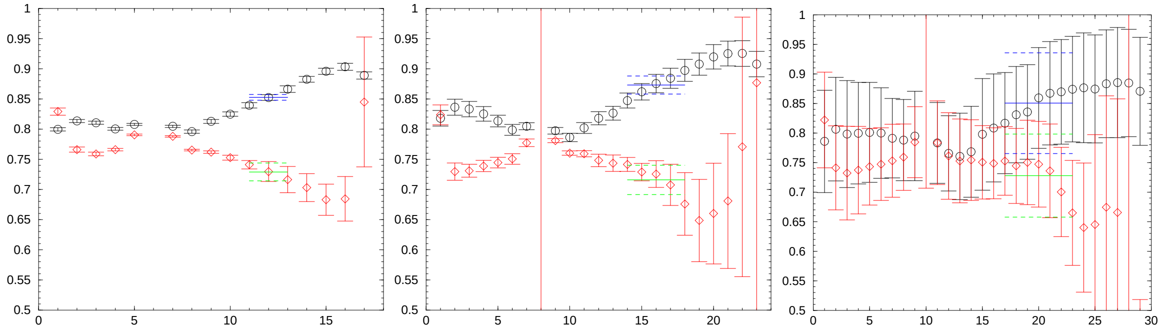

FIG. 7: x_0 dependence of $\widetilde{Z}_A(g_0, m, x_0)$ at $\beta = 1.90$ and $\theta = 0.5$ for box sizes $8^3 \times 18$ (left), $10^3 \times 24$ (middle) and $12^3 \times 30$ (right). Red diamonds and black circles are definition with or without the disconnected diagrams. Solid and dashed lines represent an expected plateau, which is given by fitting data around $x_0 = 2T/3$ by a constant. Error is estimated with the Jackknife method.

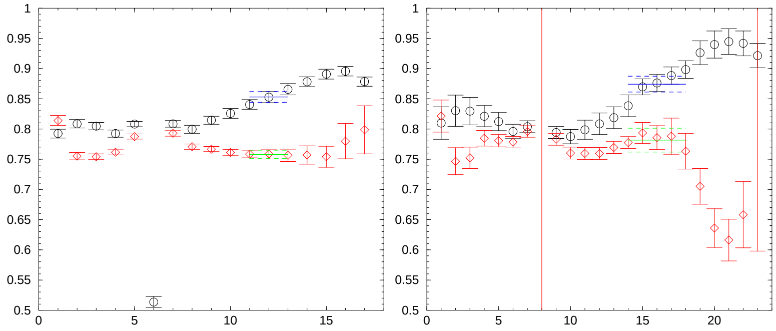

FIG. 8: x_0 dependence of $\widetilde{Z}_A(g_0, m, x_0)$ at $\beta = 1.90$ and $\theta = 0$ for box sizes $8^3 \times 18$ (left) and $10^3 \times 24$ (right).

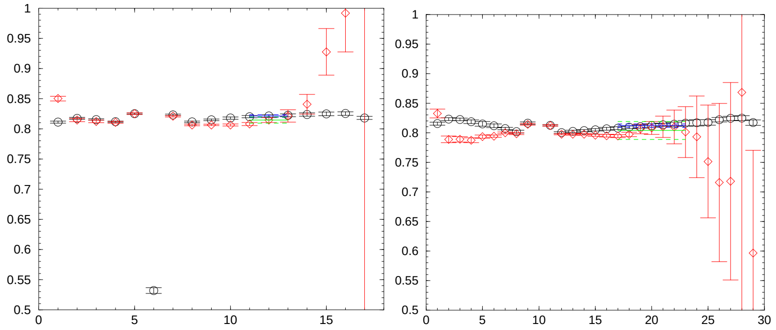

FIG. 9: x_0 dependence of $\widetilde{Z}_A(g_0, m, x_0)$ at $\beta = 2.05$ and $\theta = 0.5$ for box sizes $8^3 \times 18$ (left) and $12^3 \times 30$ (right).

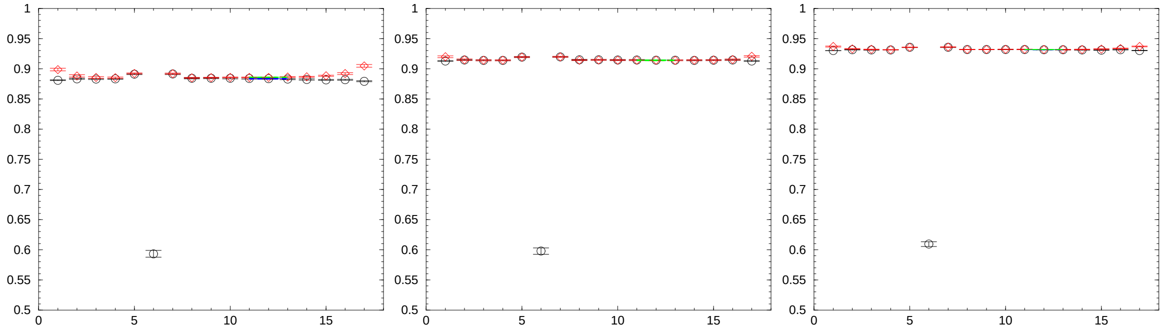

FIG. 10: x_0 dependence of $\widetilde{Z}_A(g_0, m, x_0)$ at $\beta = 3.0$ (left), 4.0 (middle) and 5.0 (right). The box size is $8^3 \times 18$ and twist angle is set to $\theta = 0.5$.

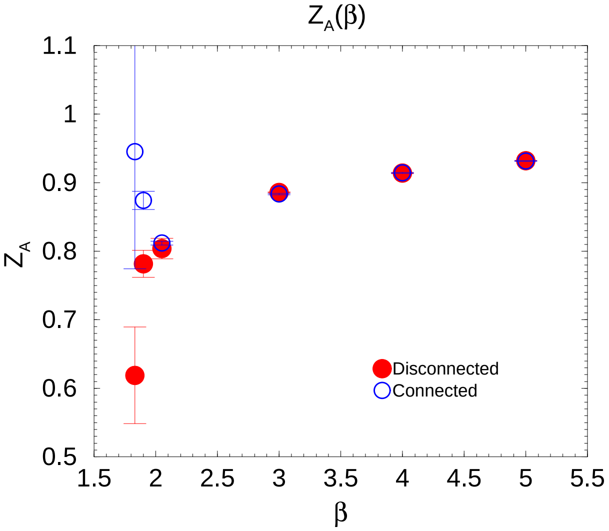

FIG. 11: β dependence of $Z_A(g_0)$ with disconnected diagrams (filled circles) and that without them (open circles).

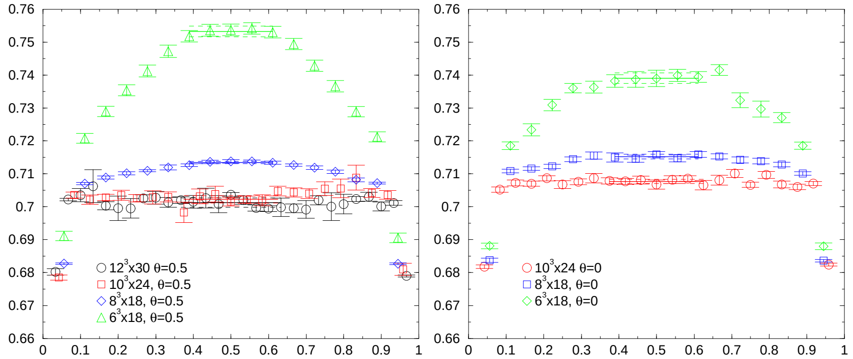

FIG. 12: x_0 dependence of $\widetilde{Z}_V(g_0, x_0)$ at $\beta = 1.83$, $\theta = 0.5$ (left) and $\theta = 0$ (right) for box sizes $6^3 \times 18$ (green triangles), $8^3 \times 18$ (blue diamonds), $10^3 \times 24$ (red squares) and $12^3 \times 30$ (black circles). Solid and dashed lines represent an expected plateau, which is given by fitting data around $x_0 = T/2$ by a constant.

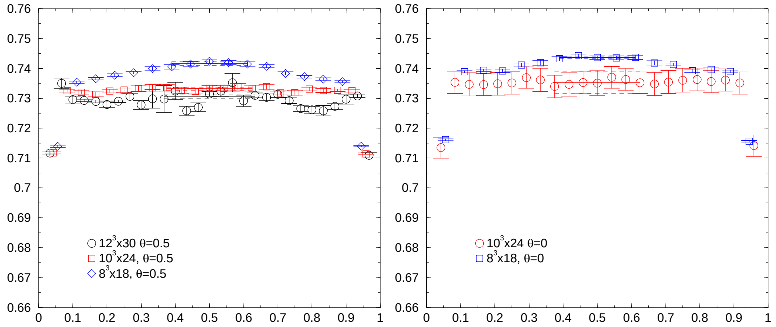

FIG. 13: x_0 dependence of $\widetilde{Z}_V(g_0, x_0)$ at $\beta = 1.90$, $\theta = 0.5$ (left) and $\theta = 0$ (right) for box sizes $8^3 \times 18$ (blue diamonds), $10^3 \times 24$ (red squares) and $12^3 \times 30$ (black circles).

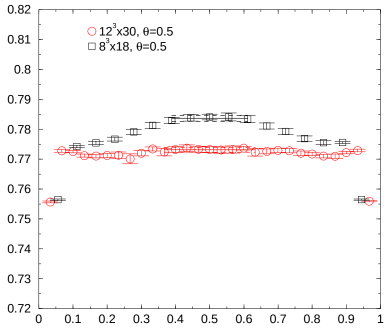

FIG. 14: x_0 dependence of $\widetilde{Z}_V(g_0, m, x_0)$ at $\beta = 2.05$ and $\theta = 0.5$ for box sizes $8^3 \times 18$ (black squares) and $12^3 \times 30$ (red circles).

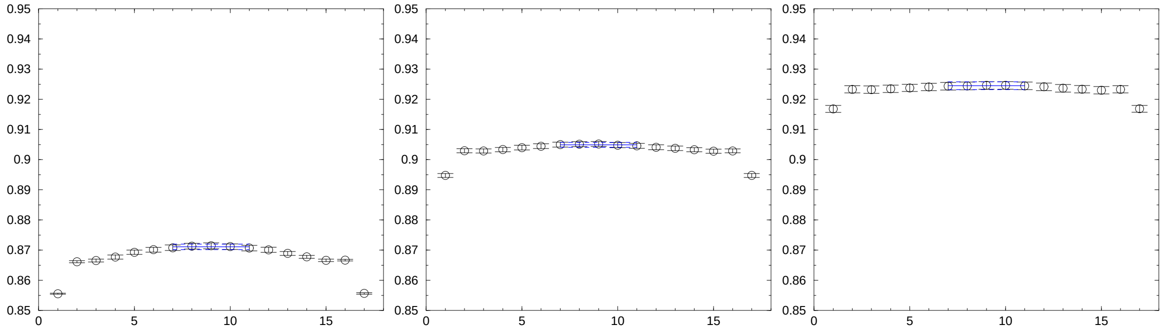

FIG. 15: x_0 dependence of $\widetilde{Z}_V(g_0, x_0)$ at $\beta = 3.0$ (left), $\beta = 4.0$ (middle) and $\beta = 5.0$ (right). A box size $8^3 \times 18$ and a value of $\theta = 0.5$ is adopted.

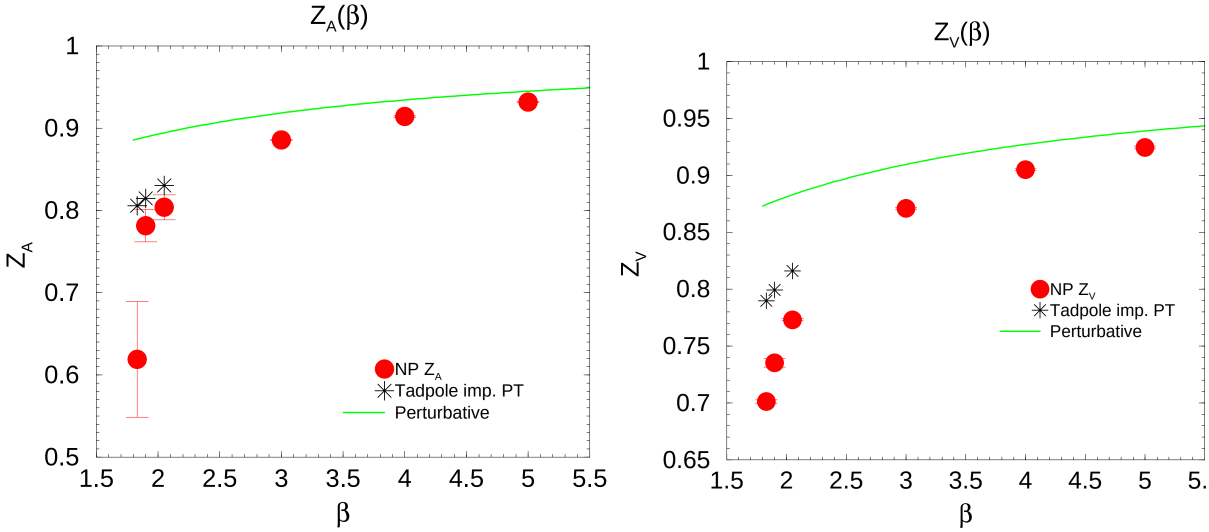

FIG. 16: β dependence of $Z_A(g_0)$ (left) and $Z_V(g_0)$ (right). Red filled circles are our non-perturbative renormalization factor. Solid line is a perturbative result at one loop. Stars are from tadpole improved perturbation theory.

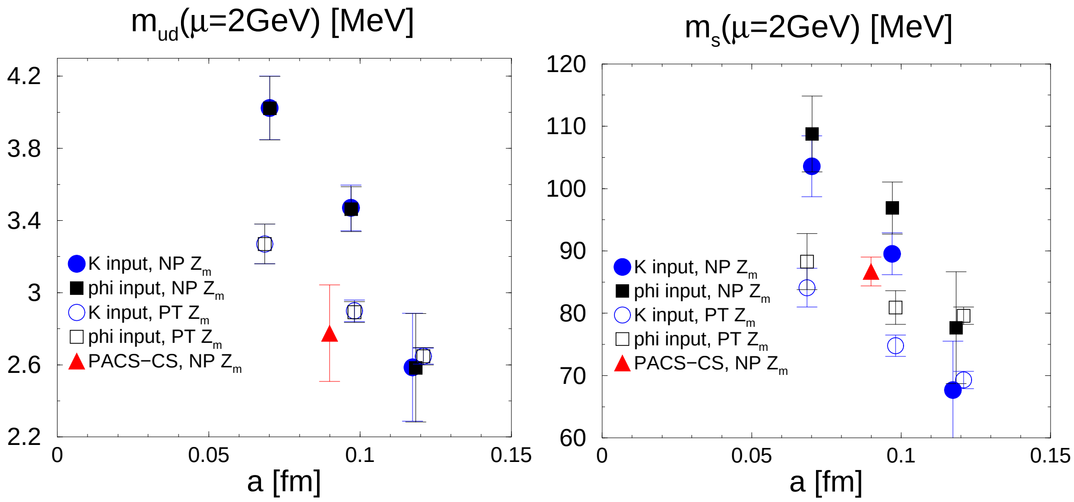

FIG. 17: Scaling behavior of $m_{ud}^{\overline{\rm MS}}$ (left) and $m_s^{\overline{\rm MS}}$ (right); filled circles and squares are from CP-PACS/JLQCD result [10], filled triangle is that of PACS-CS [12], open symbols are perturbatively renormalized masses in Ref. [10].